


Disorder-induced critical exponents near a ferromagnetic quantum critical point in $\text{Mn}_{1-x}\text{Cr}_x\text{Si}$ Ashish Kumar Mishra ^{1,*}, S. Shanmukharao Samatham ², Martin R. Lees ³ and V. Ganesan¹¹*Low Temperature Laboratory, UGC-DAE Consortium for Scientific Research, Indore 452001, MP, India*²*Department of Physics, Maharaj Vijayaram Gajapati Raj College of Engineering, Vijayaram Nagar Campus, Chintalavalasa, Vizianagaram 535005, Andhra Pradesh, India*³*Department of Physics, University of Warwick, Coventry CV4 7AL, United Kingdom*

(Received 19 December 2019; revised manuscript received 30 March 2020; accepted 30 March 2020; published 27 April 2020)

We report the observation of critical behavior in $\text{Mn}_{1-x}\text{Cr}_x\text{Si}$ ($0 \leq x \leq 1$) close to a $T = 0$ K quantum critical point, consistent with the Belitz-Kirkpatrick-Vojta (BKV) theory of disordered metallic ferromagnets. The critical exponents are in good agreement with the theoretical predictions of the BKV theory in the preasymptotic limit. A non-Fermi liquidlike behavior is seen down to 200 mK in the transport and thermodynamic properties around the critical concentration $x_C = 0.2$. Quantum criticality and self-consistency of the exponents is further confirmed using a scaling analysis of the magnetization and heat capacity data. A recovery to Fermi liquidlike behavior is displayed on moving away from the critical composition, as well as with the application of a magnetic field.

DOI: [10.1103/PhysRevB.101.144436](https://doi.org/10.1103/PhysRevB.101.144436)**I. INTRODUCTION**

Tuning a continuous phase transition towards $T = 0$ K, through some nonthermal parameters such as pressure (p), magnetic field (H) or chemical substitution (x) leads to a quantum critical point (QCP). Systems close to a QCP are of fundamental importance, as the strong electron correlations present near the QCP give rise to interesting physical phenomena such as the heavy fermion behavior in f electron-based systems, non-Fermi-liquid (NFL) behavior, and unconventional high- T_C superconductivity [1]. The conventional Hertz-Millis-Moriya theory (HMM) [2–5] predicts a continuous phase transition with mean-field exponents in the case of ferromagnetic metals near a $T = 0$ K ferromagnet to paramagnet (FM–PM) transition. However, the well-known examples of itinerant ferromagnets, namely MnSi [6], ZrZn₂ [7], and UGe₂ [8], where pressure is used as a tuning parameter to suppress ferromagnetic ordering, deviate from such behavior. Belitz, Kirkpatrick, and Vojta (BKV) demonstrated that the continuous tuning of the order parameter in sufficiently clean metallic ferromagnets is hampered through the growth of a discontinuous order parameter [9–11]. This happens due to a coupling between order parameter fluctuations with soft mode excitations present in metallic systems at relatively lower temperatures. BKV theory further suggested that a disorder induced suppression of T_C remains continuous down to $T = 0$ K [12–14]. The experimental results for the case of disorder induced FM QCP, however, are exceptionally rare [15,16].

MnSi with a low ordering temperature $T_C \sim 30$ K, is a candidate system to show a quantum phase transition (QPT) and has been studied extensively in this regard [1,6]. MnSi

is a weak itinerant helimagnet (HM) with a pitch length of around 18 nm, which in a long wavelength limit is taken as a ferromagnet [17]. It recently attracted attention because of the presence of a skyrmion phase in the H – T phase diagram below T_C [18]. However, the continuous nature of the ferromagnetic ordering in MnSi, changes towards first-order, with the application of external pressure above $p^* \sim 12$ kbar $< p < p_C$ (critical pressure $p_C \sim 14.6$ kbar), which results in a tricritical point below $T \sim 12$ K and the emergence of tricritical wings in the p – T – H phase diagram [6,19], in agreement with the theoretical predictions [9,20,21]. Nevertheless, a putative QCP under the application of a magnetic field in $\text{Mn}_{1-x}\text{Fe}_x(\text{Co}_x)\text{Si}$ [critical concentration $x_C(\text{Fe}) \sim 0.192$ and $x_C(\text{Co}) \sim 0.084$] has been reported [22]. Yet another report suggested the restoration of a QCP in $\text{Mn}_{0.85}\text{Fe}_{0.15}\text{Si}$ at a critical pressure of $p_{\text{QCP}} \sim 21$ – 23 kbar [23]. In contrast, however, a recent report disputed the emergence of a QCP in $\text{Mn}_{0.85}\text{Fe}_{0.15}\text{Si}$ with pressure [24]. Although reports [22,23] claimed the restoration of a QCP as a function of doping and pressure, the nature of the QPT in MnSi remains elusive. Also, the critical behavior down to $T = 0$ K, with doping has rarely been studied in this compound, whereas, critical behavior studies in the parent compound suggest the critical exponents of MnSi belong to the tricritical mean-field theory universality class [25,26]. The present study aims to explore the doping induced quantum phase transition and to clarify the role of disorder and the nature of a quantum phase transition in metallic ferromagnets.

In this work, we present a detailed transport and thermodynamic study across the series $\text{Mn}_{1-x}\text{Cr}_x\text{Si}$ ($0 \leq x \leq 1$). We report the observation of critical behavior in Cr doped MnSi near a FM QCP and discuss it in the light of BKV theory for disordered metallic ferromagnets. We argue that the system

*ashishkm@csr.res.in

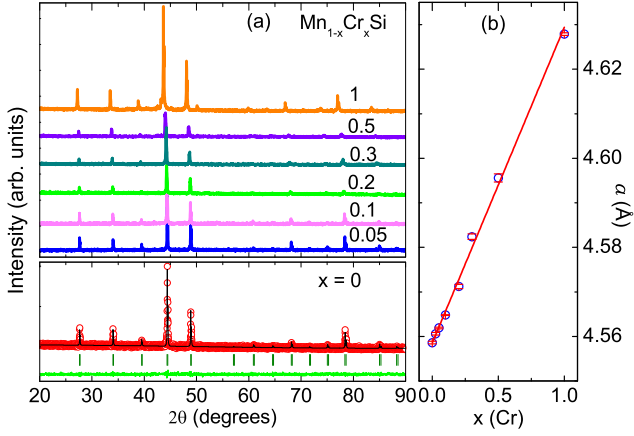


FIG. 1. (a) Room temperature XRD for different concentrations x . Rietveld refinement fit with Bragg positions for $x = 0$ is shown in the lower panel. (b) Variation of lattice parameter a as a function of x . Solid red line represents a linear fit.

is close to a doping induced ferromagnetic QCP, which is further supported through the observation of non-Fermi-liquid behavior around a critical concentration $x_C \sim 0.2$.

II. EXPERIMENTAL DETAILS

Polycrystalline samples of $\text{Mn}_{1-x}\text{Cr}_x\text{Si}$ with the nominal compositions ($x = 0, 0.025, 0.05, 0.10, 0.20, 0.30, 0.50,$ and 1.0) were prepared by arc melting and then annealed at 900°C for 48 h [27]. To confirm the phase purity, powder x-ray diffraction data were collected in a Bruker D8 Advance diffractometer. Heat capacity and electrical resistivity measurements were carried out using a Quantum Design (QD) Physical Property Measurement System (PPMS) and a dilution refrigerator. Magnetization measurements were made in a QD Magnetic Property Measurement System magnetometer with an i-Quantum insert.

III. RESULTS AND DISCUSSION

Rietveld refinement using FULLPROF software of powder x-ray diffraction data collected at room temperature in a Bruker D8 Advance diffractometer confirm the samples are single phase with a cubic $P2_13$ space group. A linear increase in the lattice parameter from $a = 4.5586(3)$ Å for MnSi to $a = 4.6279(3)$ Å for CrSi is consistent with the Vegard's law [Fig. 1(a) and 1(b)]. The lattice parameters obtained from the refinements are presented in Table I [27]. The QPT in

TABLE I. Lattice parameter and Debye temperature for different x .

Concentration (x)	a (Å)	θ_D (K)
0	4.5586(3)	508 ± 2
0.025	4.5606(3)	503 ± 2
0.05	4.5619(2)	506 ± 1
0.1	4.5648(1)	505 ± 3
0.2	4.5712(5)	502 ± 5
0.3	4.5824(6)	501 ± 7
0.5	4.5956(9)	500 ± 10
1	4.6279(3)	500 ± 11

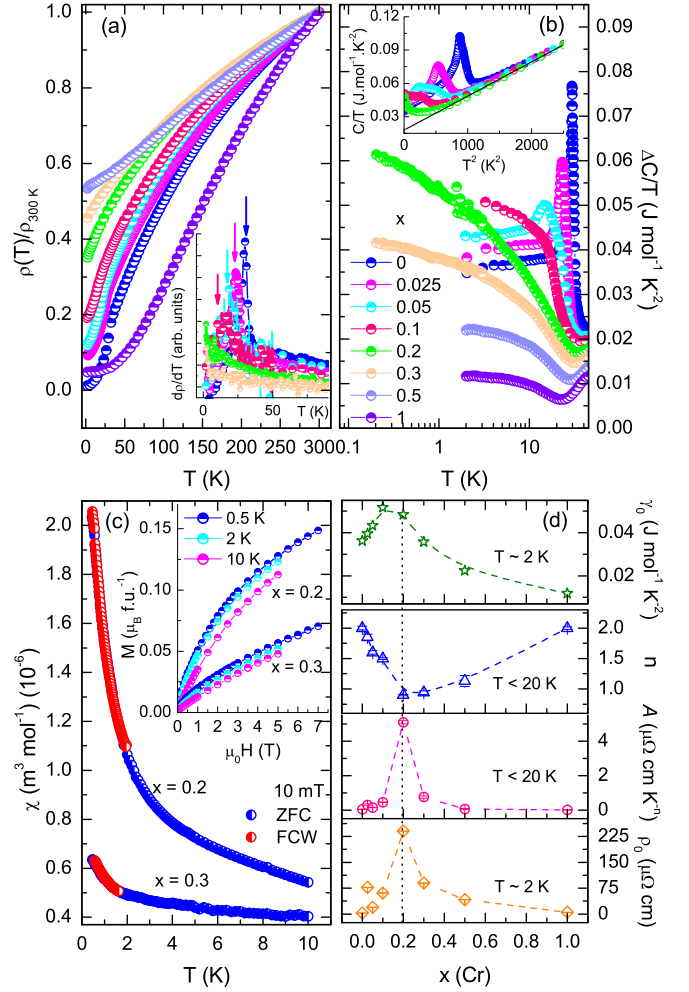


FIG. 2. (a) Normalized dc electrical resistivity $\rho(T)/\rho_{300\text{K}}$ as a function of T down to 2 K for different concentrations, x . Inset: Temperature variation of the derivative ($d\rho/dT$). The arrows mark the variation of T_C with increasing Cr concentration. (b) $\Delta C/T$ as a function of T down to 2 K and additionally for $x = 0.2$ and 0.3 down to 200 mK on a semilog scale for different x . Inset: C/T against T^2 , the black line represents the linear fit as described in the main text. (c) χ as a function of T for zero-field-cooled (ZFC) and field-cooled-warming (FCW) down to 450 mK for $x = 0.2$ and 0.3 measured in 10 mT. Inset: The corresponding M vs H at three temperatures. (d) Parameters obtained from $\rho(T)$ and $C(T)$: residual resistivity ρ_0 , exponent n , coefficient A , and γ_0 as a function of x .

$\text{Mn}_{1-x}\text{Cr}_x\text{Si}$ has been investigated using electrical resistivity $\rho(T)$ and heat capacity $C(T)$ down to 2 K. Figure 2(a) shows the temperature variation of the resistivity normalized at 300 K [$\rho(T)/\rho_{300\text{K}}$] for different x in zero magnetic field. The small anomaly at T_C (a peak in $d\rho(T)/dT$ [inset of Fig. 2(a)]) is seen to move down in temperature with increasing Cr concentration and could be observed up to $x = 0.1$. However, for $x = 0.2$, T_C could not be observed down to 0.2 K. Further, Fig. 2(b) shows $\Delta C/T$ as a function of temperature between 2 and 50 K for different x in zero magnetic field, where $\Delta C = (C - C_{\text{lattice}})$. The lattice contribution, calculated from the linear region in C/T vs T^2 of the form $C/T \sim \beta T^2$ has been subtracted separately for different x , where, the term

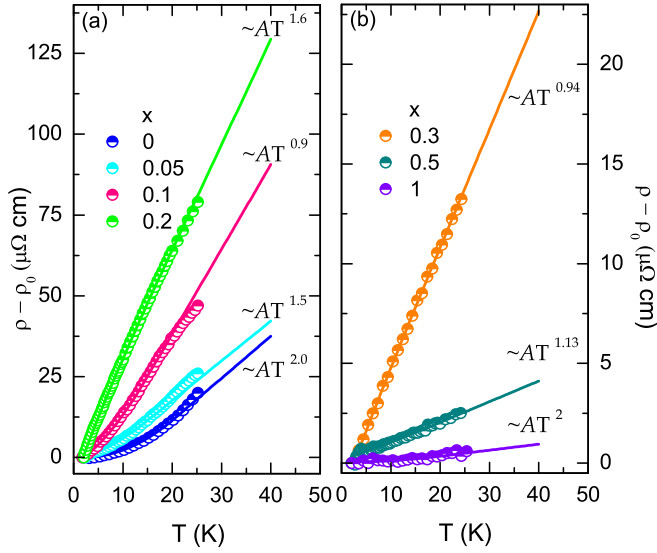


FIG. 3. (a) and (b) $\rho - \rho_0$ as a function of T for different x under zero magnetic field. The solid line represents the fit using the equation $\Delta\rho = AT^n$.

β denotes the lattice contribution. The Debye temperature obtained from the fit, using the relation $\theta_D = (5\beta/12R\pi^4)^{-1/3}$ varies between $\theta_D \sim 500$ – 508 K and is shown in Table I, [inset of Fig. 2(b)]. A well-defined peak in $\Delta C(T)/T$ for $x = 0$ can be seen at $T_C \sim 30$ K. However, with increasing x the peak broadens and vanishes above $x = 0.2$. The absence of any anomaly in measurements extended down to 0.2 K for $x = 0.2$ and 0.3 suggest the compounds remain paramagnetic for $x \geq 0.2$. Moreover, a significant low temperature rise in $\Delta C(T)/T$ for $x = 0.2$, suggests an entropy accumulation that further indicates the system is close to a QCP. Figure 2(c) shows the magnetic dc susceptibility $\chi[\equiv M/H]$ against temperature, measured at 10 mT. The $\chi(T)$ data also support the absence of a transition down to 0.45 K for $x = 0.2$ and 0.3. The reversibility of the $\chi(T)$ curves for $x = 0.2$ and 0.3 suggests there is no glassy behavior near and above the critical concentration x_C , which is common in systems with disorder [28]. The inset of Fig. 2(c) shows the magnetization M as a function of H for $x = 0.2$ and 0.3 up to 7 T. The magnetization at 2 K and 7 T for $x = 0.2$ is reduced from the parent compound MnSi [22]. Also, the $\rho(T)$ data below 20 K for different x were analyzed using: $\rho = \rho_0 + AT^n$, where ρ_0 is the residual resistivity; A and n are a coefficient and exponent, respectively (discussed below). Parameters such as ρ_0 , A , n , and Sommerfeld coefficient γ_0 obtained down to 2 K, from $\rho(T)$ and $C(T)$ data, are summarized in Fig. 2(d), which also indicates the critical concentration to be around $x_C \sim 0.2$. ρ_0 , A , and γ_0 increase with increasing x , each have a maximum at the critical concentration $x_C = 0.2$ and decrease thereafter. Correspondingly, the exponent n shows a minimum with a value of $n \sim 1$ at x_C . However, it gradually recovers to a value close to $n \sim 2$, for both the end compounds. Also, for $x_C = 0.2$, $\rho_0 \sim 240 \mu\Omega \text{ cm}$ is substantially higher than for MnSi ($\rho_0 \sim 3 \mu\Omega \text{ cm}$)

Figures 3(a) and 3(b) show the electrical resistivity ($\rho - \rho_0$) against temperature in the range 2–25 K for different

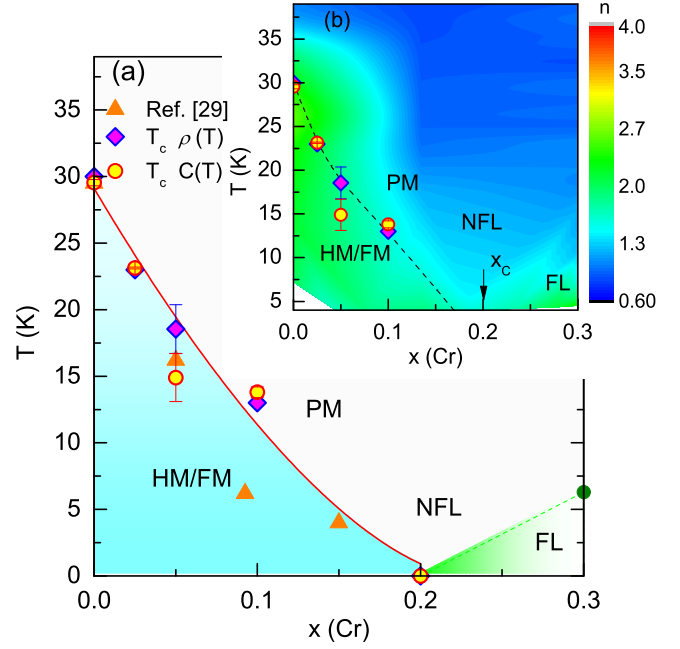


FIG. 4. (a) T - x phase diagram constructed from $\rho(T)$, $C(T)$ and Ref. [29]. The data points were fitted with the relation $T_C \sim (x_C - x)^z$ shown with the solid red line. The green dashed line marks the crossover from NFL to FL behavior. (b) Contour plot showing the variation of the exponent n across the T - x phase diagram.

concentrations of x . Solid lines are fits to a term proportional to $\Delta\rho = AT^n$. The curves up to $x \sim 0.1$ were fitted below the observed T_C . However, the curves for x above 0.2 were fitted in the range 2–20 K. Close to the critical concentration the exponent shows an almost linear in temperature behavior. Such a linear resistivity in temperature is unusual as compared to pressure dependent studies in MnSi [6], where the observed exponent is close to $n \sim 3/2$. However, the exponent n starts to increase gradually and recovers its value of $n \sim 2$ for the end compounds MnSi and CrSi.

A T - x phase diagram incorporating the important parameters determined in the present study is shown in Figs. 4(a) and 4(b). The phase diagram is constructed using T_C as inferred from $\rho(T)$ and $C(T)$. T_C is seen to vanish completely for a critical concentration around $x_C = 0.2$ and results in a QPT. Figure 4(b) shows the variation of the exponent n from the $\rho(T)$ data. A value of n between 0.6 and 1.5 spans the PM region and prevails near the quantum critical region down to the lowest temperature. However, a value closer to 2 is seen away from the critical region, i.e., in the ordered region as well as at lowest temperatures for $x \geq 0.3$.

Furthermore, Fig. 5 shows the variation of the magnetic Grüneisen ratio, $\Gamma_H = -(dM/dT)/C$, [30] as a function of temperature for $x = 0.2$. The Γ_H diverges with a power law down to 500 mK with $\Gamma_H \sim T^{-2}$. Such diverging behavior of Γ_H is seen to be satisfied for systems at a zero field QCP [31,32].

In addition, the magnetic field is found to tune the NFL behavior towards FL behavior in various $3d$ and $4f$ compounds [1]. The magnetic field induced NFL to FL crossover for $x = 0.2$ is shown in Figs. 6(a) and 6(b). Figure 6(a) shows

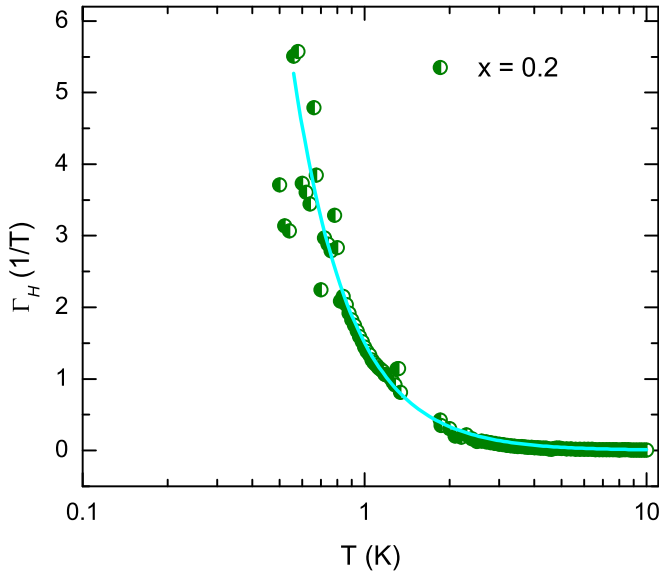


FIG. 5. Magnetic Grüneisen ratio, Γ_H as a function of temperature, for the critical concentration $x = 0.2$. The line represents a power law fit.

the variation of the coefficient of resistivity A and exponent n with magnetic field for $x = 0.2$. The value of A decreases in the field of 12 T. Similarly, the value of the exponent n recovers to a value of $n \sim 1.5$ with the application magnetic field of 12 T. Furthermore, the Sommerfeld coefficient γ_0 [Fig. 6(b)] also decreases with the application of magnetic field and seems to saturate at and above 12 T. A clear decrease in the value of A and γ_0 suggests the suppression of critical spin fluctuations in a magnetic field and further supports NFL to FL crossover upon the application of a magnetic field for $x = 0.2$ [1,27,33].

For $x = 0.2$, Figs. 7(a) and 7(b) show $\Delta C/T$ and χ versus temperature. A negative logarithmic behavior $-\ln T$ for almost a decade of temperature, 0.2 to 2 K for $\Delta C(T)/T$ and 0.45

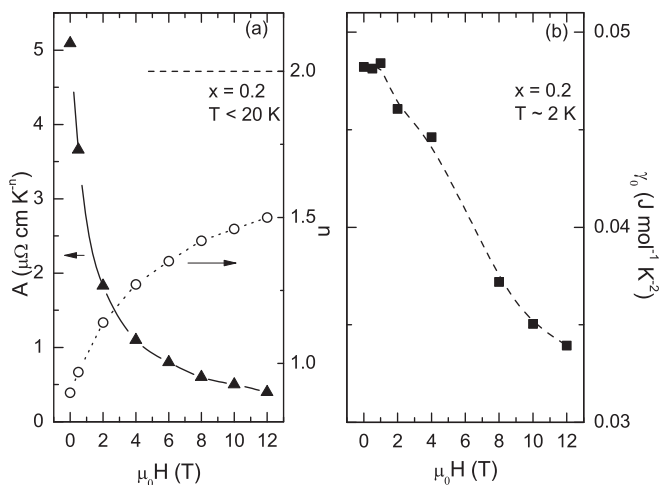


FIG. 6. (a) Electrical resistivity coefficient A (left axis) and n (right axis) and (b) Sommerfeld coefficient γ_0 as a function of $\mu_0 H$ up to 12 T. Dashed line in (a) marks the value of $n = 2$.

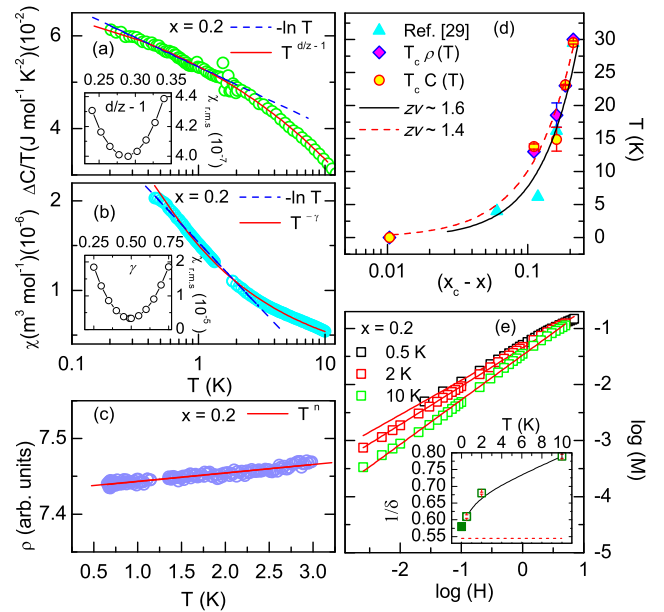


FIG. 7. (a) $\Delta C/T$ and (b) χ as a function of T (on a semilog scale). The solid red line represents the power-law fit. The dashed blue line represents a $-\ln T$ behavior. (c) $\rho(T)$ in the range 0.5–3 K, where the solid red line represents a linear fit. (d) Variation of T_C with $x_C - x$ (on a semilog scale), where the solid and dashed lines represent fits. (e) $M-H$ isotherms plotted as the $\log M$ vs $\log H$, where the lines are the linear fits. Inset: $1/\delta$ as a function of temperature (closed symbols) and extrapolated to 0 K (open symbols). The red dotted line marks the value in the preasymptotic limit.

to 4 K for $\chi(T)$, respectively, suggests a non-Fermi-liquid behavior. Additionally, the data below 10 K could also be described using a power law. The critical contribution to $\Delta C(T)/T$ in the form $\sim T^{d/z-1}$, provides a value of $d/z = 1.28 \pm 0.02$, where d and z are the dimensionality and dynamical exponent, respectively. For $d = 3$, z is found to be $z \sim 2.34 \pm 0.02$ [34]. Similarly, $\chi(T)$ below $T \sim 10$ K, returned a value of the critical exponent $\gamma \sim 0.49 \pm 0.01$. Only the final values of the exponents that resulted in the minimum χ_{rms} (root-mean-square deviation) were considered [34]. A non-Fermi-liquid behavior is also seen in the resistivity, where $\rho(T)$ versus temperature for $x = 0.2$, shows a linear behavior from 3 to 0.5 K [Fig. 7(c)]. These results suggest that $x = 0.2$ is close to the critical concentration. Consider now the dependence of T_C on the distance from the critical concentration x_C , which is important in determining the spatial correlation length exponent ν . The variation of T_C with x is fitted with a term proportional to $T_C \sim (x_C - x)^{z\nu}$ and is shown in Fig. 7(d). Here, the correlation length exponent ν is related to correlation length ξ as: $\xi \sim |x - x_C|^{-\nu}$ and z is related to the divergence of the correlation time τ as: $\xi_\tau \sim \xi^z$. The obtained value of $z\nu \sim 1.4$ is different from the value of $4/5$ for the case of Hertz type disordered ferromagnetic QPT. However, it is in close agreement with a value of $z\nu = 1.6$ provided by the BKV theory in the preasymptotic limit [35]. The fit using the value from BKV theory is also shown in the Fig. 7(d), which seems to follow the data quite well. Furthermore, the value $z \sim 2.34$ gives the value of $\nu \sim 0.6$.

TABLE II. Critical exponents obtained in the present work compared with the exponents expected from BKV theory in the asymptotic and preasymptotic limits [35].

Critical exponents	Asymptotic limit	Preasymptotic limit	Present
β	1	0.75	0.8
δ	1.5	1.83	1.63
γ	0.5	0.625	0.5
ν	1	0.6	0.6
z	2	2.67	2.34

The values provided by the BKV theory in the preasymptotic limit of $z = 2.67$ and $\nu = 0.6$ are in accord with the values obtained here. Figure 7(e) shows $\log M$ as a function of $\log H$. The slope of the linear region in $\log H$ provides another important exponent in the form of $1/\delta$. The values of $1/\delta$ as a function of temperature are shown in the inset of Fig. 7(e). The value at 0.5 K is $\delta \sim 1.63 \pm 0.01$, which on extrapolating linearly to $T = 0$ K gives $\delta \sim 1.7$, again in line with the $\delta \sim 1.83$ from BKV theory. Nonetheless, a similar value of δ has been reported in Refs. [15,34,36,37]. Subsequently, Widom's law, $\gamma = \beta(\delta - 1)$, then gives $\beta = 0.8$. Table II compares the obtained exponents in the present case with the BKV theory. Some exponents to within error are equally valid in the asymptotic limit of BKV theory. However, considering the difficulty in controlling the distance from the critical concentration, in the case of doping, the exponents in the preasymptotic limit explain the present results better.

To confirm the quantum criticality and self-consistency of the exponents obtained, we chose to perform a critical scaling analysis. In the case of quantum criticality, the thermodynamic and magnetic properties are described through dynamical scaling, with static and dynamics coupled together.

Assuming, only one dominant critical time scale z at the QCP, and provided hyperscaling holds, one can write the free energy as [34]

$$f(T, H) = b^{-(d+z)} f(b^z T, b^{\beta\delta/\nu} H), \quad (1)$$

where b is an arbitrary scale factor and $f(b^z T, b^{\beta\delta/\nu} H)$ is a universal scaling function. z and $\beta\delta/\nu$ denote the scaling exponents related to T and H , respectively. Defining the critical heat capacity and magnetization in terms of the free energy

$$C_{cr}(T, H) = -T(\partial^2 f / \partial T^2) = b^{-d} C_{cr}(b^z T, b^{\beta\delta/\nu} H), \quad (2)$$

$$M(T, H) = -(\partial f / \partial H) = b^{\beta\delta/\nu - (d+z)} M(b^z T, b^{\beta\delta/\nu} H), \quad (3)$$

which gives the critical scaling functions as

$$C_{cr}(T, H) = T^{d/z} \Psi(H/T^{\beta\delta/z\nu}), \quad (4)$$

$$M(T, H) = T^{\beta/\nu z} \Phi(H/T^{\beta\delta/z\nu}). \quad (5)$$

Figure 8(a) shows the temperature–field scaling plot of $[C(T, H) - C(T, 0)]/T^{d/z}$ against $H/T^{\beta\delta/z\nu}$. Utilizing Eq. (4) the scaling results in a collapse onto a single curve over more than three orders in $\beta\delta/\nu z$. Likewise using Eq. (5) the mag-

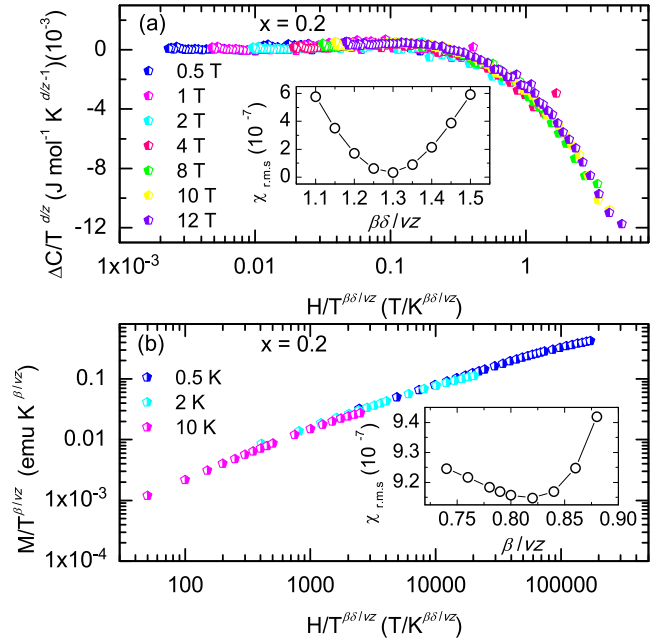


FIG. 8. (a) Scaling of heat capacity and (b) magnetization as a function of H and T . Inset: χ_{rms} against $\beta\delta/\nu z$ and $\beta/\nu z$ in (a) and (b), respectively.

netization data at different temperatures are seen to collapse onto a single curve over more than three orders of magnitude in $\beta\delta/\nu z$ [Fig. 8(b)]. The values of $\beta\delta/\nu z \sim 1.30 \pm 0.10$ and $\beta/\nu z \sim 0.82 \pm 0.05$, which resulted in a minimum in χ_{rms} against d/z and $\beta\delta/\nu z$ were considered. The collapse of data onto a single universal curve suggests the validity of the exponents and the quantum criticality, which is in good agreement with other reports [15,16,34,36–38]. Also, the ratio of the two exponents $\beta\delta/\nu z$ and $\beta/\nu z \sim 1.59$ is in agreement with the value of $\delta \sim 1.63$ obtained above.

The unusual exponents obtained, however, cannot be resolved under the HMM theory, which suggests the upper critical dimension, d_C^+ for the mean-field theory to be valid in the case of dirty ferromagnets is $d_C^+ = 0$. Conversely, the validity of the hyperscaling suggests that the present system is below the upper critical dimension. Nevertheless, the exponents are in good agreement with the BKV theory for disordered ferromagnets in the preasymptotic limit and the system could be reconciled excellently with the BKV theory. The disorder and inhomogeneity in these systems play a crucial role in determining the ultimate fate of the QCP [39] and external perturbations may lead to phase separation, as reported for MnSi and $\text{Sr}_{1-x}\text{Ca}_x\text{RuO}_3$ [40]. However, phase separation has been discarded based on the critical analysis study in $\text{Sr}_{1-x}\text{Ca}_x\text{RuO}_3$ [34], though the anomalous exponents observed cannot be reconciled with any known theory of a FM QCP.

Additionally, Griffiths or glassy behavior has also been reported with an increase in disorder in the case of $\text{Ni}_{1-x}\text{V}_x$ [41], $\text{CePd}_{1-x}\text{Rh}_x$ [42], and $\text{Mn}_{1-x}\text{Co}_x\text{Si}$ [28]. We note that, with induced disorder, the possibility of the Griffiths phase cannot be discarded completely, as the exponents obtained in the present case $\gamma \sim 0.5 \approx \alpha \sim 0.6$ are approximately related in a manner discussed in Ref. [41], where, $M/H \sim T^{-\gamma}$ and $M \sim H^\alpha$ with $1 - \gamma = \alpha$. Moreover, theoretically it

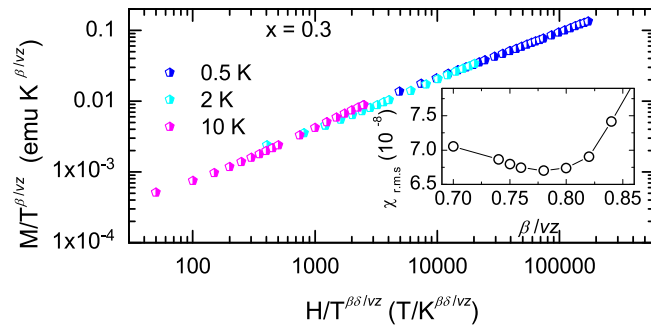


FIG. 9. Scaling of magnetization as a function of H and T for the concentration $x = 0.3$. Inset: χ_{rms} against $\beta/\nu z$.

has been shown that the critical behavior is expected to be present in addition to any Griffiths phase effects, and that the two will be independent [35]. Studies further suggested that the Griffiths phase effects cannot modify the critical behavior [43,44]. To further confirm the critical behavior for $x = 0.3$, we have performed the universal scaling (Fig. 9) incorporating the magnetization data using the similar critical exponents from $x = 0.2$. The scaling results in a clear collapse onto a single curve over more than three orders in H/T . However,

the role of Griffiths phase in QCP is subtle and must be investigated in future studies, very close to x_c .

IV. SUMMARY

Summarizing, the present study across the $\text{Mn}_{1-x}\text{Cr}_x\text{Si}$ series, reveals a QCP as a function of doping and shows a non-Fermi-liquid behavior at the critical concentration $x_c = 0.2$. A detailed critical scaling analysis for the critical composition has unambiguously established a disorder induced FM QCP in $\text{Mn}_{1-x}\text{Cr}_x\text{Si}$. To further clarify the role of disorder in QCP, studies with doping levels closer to the critical concentration will be performed.

ACKNOWLEDGMENTS

The authors thank the Director and Centre-Director, UGC-DAE CSR, Indore for their encouragement, the staff and students of LTL and Cryogenics for their support, especially Er. P. Saravanan and Dr. R. Venkatesh. A.K.M. thanks CSIR, India for SRF [File No.:09/926(0011)2K18]. S.S.S acknowledges financial support from UGC-DAE CSR, Indore (CSR-IC-256/2017-18/1337) and SERB (TAR/2018/000454). DST, India is thanked for their initial support in setting up the 14 T PPMS at CSR Indore.

- [1] G. R. Stewart, *Rev. Mod. Phys.* **73**, 797 (2001).
- [2] J. A. Hertz, *Phys. Rev. B* **14**, 1165 (1976).
- [3] A. J. Millis, *Phys. Rev. B* **48**, 7183 (1993).
- [4] R. Konno and T. Moriya, *J. Phys. Soc. Jpn.* **56**, 3270 (1987).
- [5] T. Moriya, *Spin Fluctuations in Itinerant Electron Magnetism* (Springer-Berlin, New York, 1985).
- [6] C. Pfleiderer, S. R. Julian, and G. G. Lonzarich, *Nature (London)* **414**, 427 (2001).
- [7] M. Uhlarz, C. Pfleiderer, and S. M. Hayden, *Phys. Rev. Lett.* **93**, 256404 (2004).
- [8] C. Pfleiderer and A. D. Huxley, *Phys. Rev. Lett.* **89**, 147005 (2002).
- [9] D. Belitz, T. R. Kirkpatrick, and T. Vojta, *Phys. Rev. Lett.* **82**, 4707 (1999).
- [10] T. R. Kirkpatrick and D. Belitz, *Phys. Rev. B* **85**, 134451 (2012).
- [11] A. V. Chubukov, C. Pépin, and J. Rech, *Phys. Rev. Lett.* **92**, 147003 (2004).
- [12] T. R. Kirkpatrick and D. Belitz, *Phys. Rev. B* **53**, 14364 (1996).
- [13] D. Belitz, T. R. Kirkpatrick, M. T. Mercaldo, and S. L. Sessions, *Phys. Rev. B* **63**, 174427 (2001).
- [14] D. Belitz, T. R. Kirkpatrick, M. T. Mercaldo, and S. L. Sessions, *Phys. Rev. B* **63**, 174428 (2001).
- [15] K. Huang, S. Eley, P. F. S. Rosa, L. Civale, E. D. Bauer, R. E. Baumbach, M. B. Maple, and M. Janoschek, *Phys. Rev. Lett.* **117**, 237202 (2016).
- [16] B. C. Sales, K. Jin, H. Bei, J. Nichols, M. F. Chisholm, A. F. May, N. P. Butch, A. D. Christianson, and M. A. McGuire, *npj Quant. Mater.* **2**, 33 (2017).
- [17] Y. Ishikawa, K. Tajima, D. Bloch, and M. Roth, *Solid State Commun.* **19**, 525 (1976).
- [18] S. Mühlbauer, B. Binz, F. Jonietz, C. Pfleiderer, A. Rosch, A. Neubauer, R. Georgii, and P. Böni, *Science* **323**, 915 (2009).
- [19] C. Pfleiderer, G. J. McMullan, S. R. Julian, and G. G. Lonzarich, *Phys. Rev. B* **55**, 8330 (1997).
- [20] D. Belitz, T. R. Kirkpatrick, and J. Rollbühler, *Phys. Rev. Lett.* **94**, 247205 (2005).
- [21] V. Taufour, D. Aoki, G. Knebel, and J. Flouquet, *Phys. Rev. Lett.* **105**, 217201 (2010).
- [22] A. Bauer, A. Neubauer, C. Franz, W. Münzer, M. Garst, and C. Pfleiderer, *Phys. Rev. B* **82**, 064404 (2010).
- [23] T. Goko, C. J. Arguello, A. Hamann, T. Wolf, M. Lee, D. Reznik, A. Maisuradze, R. Khasanov, E. Morenzoni, and Y. J. Uemura, *npj Quant. Mater.* **2**, 44 (2017).
- [24] A. E. Petrova, S. Y. Gavrilkin, D. Menzel, and S. M. Stishov, *Phys. Rev. B* **100**, 094403 (2019).
- [25] L. Zhang, D. Menzel, C. Jin, H. Du, M. Ge, C. Zhang, L. Pi, M. Tian, and Y. Zhang, *Phys. Rev. B* **91**, 024403 (2015).
- [26] S. S. Samatham and V. Ganesan, *Phys. Rev. B* **95**, 115118 (2017).
- [27] A. K. Mishra, M. Krishnan, D. Singh, S. S. Samatham, M. Gangrade, R. Venkatesh, and V. Ganesan, *J. Magn. Magn. Mater.* **448**, 130 (2018).
- [28] J. Teyssier, E. Giannini, V. Guritanu, R. Viennois, D. van der Marel, A. Amato, and S. N. Gvasaliya, *Phys. Rev. B* **82**, 064417 (2010).
- [29] E. Achi, H. Al-Kanani, J. Booth, M. Costa, and B. Lebech, *J. Magn. Magn. Mater.* **177**, 779 (1998).
- [30] L. Zhu, M. Garst, and A. Rosch, and Q. Si, *Phys. Rev. Lett.* **91**, 066404 (2003).
- [31] Y. Matsumoto, S. Nakatsuji, K. Kuga, Y. Karaki, N. Horie, Y. Shimura, T. Sakakibara, A. H. Nevidomskyy, and P. Coleman, *Science* **331**, 316 (2011).

- [32] Y. Tokiwa, J. J. Ishikawa, S. Nakatsuji, and P. Gegenwart, *Nat. Mater.* **13**, 356 (2014).
- [33] S. S. Samatham, S. Yadam, D. Singh, and V. Ganesan, *J. Magn. Magn. Mater.* **418**, 289 (2016).
- [34] C. L. Huang, D. Fuchs, M. Wissinger, R. Schneider, M. C. Ling, M. S. Scheurer, J. Schmalian, and H.v. Löhneysen, *Nat. Commun.* **6**, 8188 (2015).
- [35] T. R. Kirkpatrick and D. Belitz, *Phys. Rev. Lett.* **113**, 127203 (2014).
- [36] E. D. Bauer, V. S. Zapf, P.-C. Ho, N. P. Butch, E. J. Freeman, C. Sirvent, and M. B. Maple, *Phys. Rev. Lett.* **94**, 046401 (2005).
- [37] N. P. Butch and M. B. Maple, *Phys. Rev. Lett.* **103**, 076404 (2009).
- [38] S. Pandey, V. Siruguri, and R. Rawat, *Phys. Rev. B* **98**, 155129 (2018).
- [39] Y. Sang, D. Belitz, and T. R. Kirkpatrick, *Phys. Rev. Lett.* **113**, 207201 (2014).
- [40] Y. J. Uemura, T. Goko, I. M. Gat-Malureanu, J. P. Carlo, P. L. Russo, A. T. Savici, A. Aczel, G. J. MacDougall, J. A. Rodriguez, G. M. Luke, S. R. Dunsiger, A. McCollam, J. Arai, C. Pfleiderer, P. Böni, K. Yoshimura, E. Baggio-Saitovitch, M. B. Fontes, J. Larrea, Y. V. Sushko, and J. Sereni, *Nat. Phys.* **3**, 29 (2007).
- [41] S. Ubaid-Kassis, T. Vojta, and A. Schroeder, *Phys. Rev. Lett.* **104**, 066402 (2010).
- [42] T. Westerkamp, M. Deppe, R. Küchler, M. Brando, C. Geibel, P. Gegenwart, A. P. Pikul, and F. Steglich, *Phys. Rev. Lett.* **102**, 206404 (2009).
- [43] M. Brando, and D. Belitz, F. M. Grosche, and T. R. Kirkpatrick, *Rev. Mod. Phys.* **88**, 025006 (2016).
- [44] T. Vojta and J. A. Hoyos, *Phys. Rev. Lett.* **112**, 075702 (2014).